Author Manuscript

Author Manuscript

Author Manuscript

Author Manuscript

HHS Public Access

Author manuscript

Nanotoxicology. Author manuscript; available in PMC 2018 April 01.

Published in final edited form as:

Nanotoxicology. 2017 April ; 11(3): 313–326. doi:10.1080/17435390.2017.1299888.

Mapping Differential Cellular Protein Response of Mouse Alveolar Epithelial Cells to Multi-Walled Carbon Nanotubes as a Function of Atomic Layer Deposition Coating

Gina M. Hilton[1], **Alexia J. Taylor**[1], **Salik Hussain**[2], **Erinn C. Dandley**[4], **Emily H. Griffith**[3], **Stavros Garantziotis**[2], **Gregory N. Parsons**[4], **James C. Bonner**[1], and **Michael S. Bereman**[1]

[1]Toxicology Program, Department of Biological Sciences, North Carolina State University, Raleigh, NC

[2]Clinical Research Unit, National Institute of Environmental Health Sciences/National Institute of Health, Research Triangle Park, NC

[3]Department of Statistics, North Carolina State University, Raleigh, NC

[4]Department of Chemical and Biomolecular Engineering, North Carolina State University, Raleigh, NC

Abstract

Carbon nanotubes (CNTs), a prototypical engineered nanomaterial, have been increasingly manufactured for a variety of novel applications over the past two decades. However, since CNTs possess fiber-like shape and cause pulmonary fibrosis in rodents, there is concern that mass production of CNTs will lead to occupational exposure and associated pulmonary diseases. The aim of this study was to use contemporary proteomics to investigate the mechanisms of cellular response in E10 mouse alveolar epithelial cells *in-vitro* after exposure to multi-walled CNTs (MWCNTs) that were functionalized by atomic layer deposition (ALD). ALD is a method used to generate highly uniform and conformal nanoscale thin-film coatings of metals to enhance novel conductive properties of CNTs. We hypothesized that specific types of metal oxide coatings applied to the surface of MWCNTs by ALD would determine distinct proteomic profiles in mouse alveolar epithelial cells *in-vitro* that could be used to predict oxidative stress and pulmonary inflammation. Uncoated (U)-MWCNTs were functionalized by ALD with zinc oxide (ZnO) to yield Z-MWCNTs or aluminum oxide (Al_2O_3) to yield A-MWCNTs. Significant differential protein expression was found in the following critical pathways: mTOR/eIF4/p70S6K signaling and Nrf-2 mediated oxidative stress response increased following exposure to Z-MWCNTs, interleukin-1 signaling increased following U-MWCNT exposure, and inhibition of angiogenesis by thrombospondin-1, oxidative phosphorylation, and mitochondrial dysfunction increased following A-MWCNT exposure. This study demonstrates that specific types of metal oxide thin film coatings applied by ALD produce distinct cellular and biochemical responses related to lung inflammation and fibrosis compared to uncoated MWCNT exposure *in-vitro*.

*Author for Correspondence: Michael S. Bereman, Ph.D., Department of Biological Sciences, Center for Human Health and the Environment, North Carolina State University, Raleigh, NC, Phone: 919.515.8520, michaelbereman@ncsu.edu.

Author Manuscript Author Manuscript Author Manuscript Author Manuscript

Keywords

Carbon Nanotube; Label-Free Proteomics; Pulmonary Fibrosis; Toxicoproteomics

Introduction

Carbon nanotubes (CNTs), nanomaterials resembling rolled sheets of graphene, are quickly emerging in the field of nanotechnology due to extraordinary applications in electronics, engineering, and medicine [1]. Multi-walled (MW) CNTs are used primarily to increase the tensile strength of a variety polymers in the electronics and semi-conductor industry [2]. MWCNTs are being developed for a wide range of applications including electronics, energy storage and incorporation into polymers [3, 4]. For some applications, surface modification or thin film coatings on the MWCNTs can add enhanced functionality to improve electronic or physical performance. Atomic layer deposition, ALD, is a novel process to generate highly uniform and conformal nanoscale thin-film coatings, including: metal oxides, metals, and hybrid metal/organic materials [5–7]. While CNTs are quickly evolving for numerous applications, the fact still remains that they possess fiber-like physical characteristics similar to asbestos [8], a material that has resulted in hundreds of thousands of cases of pulmonary fibrosis and mesothelioma [9]. In addition to their fiber-like structure, CNTs have been reported to exhibit varying degrees of toxicity depending on factors including: length, width, residual metal content, agglomeration status, and surface functionalization, which are thought to contribute to pulmonary inflammation and disease [10].

Pulmonary fibrosis is a fatal disease that is characterized by scaring of the lung tissue, which ultimately results in impaired lung function [11]. Rodent studies have shown that pulmonary exposure to SWCNTs or MWCNTs by inhalation, instillation, or oropharyngeal aspiration (OPA) results in pulmonary fibrosis [12]. In addition to *in vivo* studies of fibrogenesis in experimental animals, *in vitro* studies have also shown that MWCNT exposure induces the production of growth factors and cytokines involved in the fibrogenic response, which is largely initiated through oxidative stress mechanisms [13, 14]. In particular, the alveolar epithelium is the primary target of CNT deposition in the distal lung and therefore alveolar epithelial cells are an appropriate cell type to elucidate mechanisms of CNT-induced lung disease *in vitro* [15]. We previously investigated the pulmonary toxicity of ALD-functionalized MWCNTs, coated with either aluminum oxide (A-MWCNT) or zinc oxide (Z-MWCNT), in mice *in vivo* after delivery to the lungs by oropharyngeal aspiration [16, 17]. In these studies, we compared *in vivo* induction of pro-inflammatory and pro-fibrogenic cytokines in the bronchoalveolar lavage fluid (BALF) from mice with production of cytokines by human THP-1 monocytic cells. A-MWCNT caused less pulmonary fibrosis in mice compared to uncoated MWCNTs (U-MWCNTs) and caused reduced levels of pro-inflammatory and pro-fibrogenic cytokines (interleukin-6, tumor necrosis factor-alpha, osteopontin) in THP-1 cells *in vitro* [16]. Z-MWCNTs caused a similar degree of pulmonary fibrosis compared to U-MWCNT, but caused marked acute lung and systemic inflammation in mice with high levels of interleukin-6 that corresponded to exaggerated levels of interleukin-6 induced by Z-MWCNTs in THP-1 cells *in vitro* [17]. These studies highlighted

Author Manuscript Author Manuscript Author Manuscript Author Manuscript

vastly different pathologic and molecular responses to different ALD-MWCNTs in mice that could be partly predicted by cytokine profiles from THP-1 cells, but were limited by the measurement of only a few cytokine biomarkers of inflammation and fibrosis. To better understand underlying cellular mechanisms of response to various ALD-coated MWCNTs, cutting-edge tools emerging in measurement science, i.e. liquid chromatography tandem mass spectrometry (LC-MS/MS), offer superior advantages to identify a large number of proteins in an unbiased manner to rapidly elucidate toxicity of functionalized MWCNTs.

Mass spectrometry based proteomics is a powerful 'omics' method used in measurement science to evaluate global changes in proteins; examples include: analysis of post-translational modifications (PTMs), identification of protein-protein interaction (PPI), and changes in protein abundance due to system perturbation. Recent reports have suggested that the proteome serves as a direct mediator between toxicants and the resulting cellular response to insult [18]. Currently, LC-MS/MS is a prevailing analytical tool used in proteomics due to its high sensitivity and unparalleled molecular specificity. Fortunately, proteomics can be used to generate large amounts of data that represent the cellular state by examining changes in protein expression upon toxicant exposure. Due to the large amount of data generated in proteomic experimentation, enrichment analyses, such as pathway analysis, are helpful to find biological changes that result from differential protein expression [19]. More specifically, enrichment analysis serves to identify over-represented groups of proteins that can be further associated with a specific pathway or function. Changes in biological pathways that are associated with groups of differentially expressed proteins can serve as a signature to specific perturbations in a biological system. Enriched pathways help to highlight proteins of interest for further examination, and ultimately identify markers that can help predict toxicant response.

In this study, we postulated that specific types of metal oxide coatings applied to the surface of MWCNTs by ALD would determine distinct proteomic profiles in mouse alveolar epithelial cells *in vitro* that could be used to predict oxidative stress and pulmonary inflammation. Herein, we investigated changes in protein expression as a function of MWCNT coating by using a combination of shotgun and targeted proteomic methods. The E10 cell line, isolated from normal mouse alveolar epithelial tissue, was used to create an *in vitro* model of MWCNT exposure [20]. The following pathways were enriched for significant differences in protein expression as a function of MWCNT coating type: mTOR signaling from Z-MWCNT exposure, mitochondrial dysfunction and oxidative phosphorylation signaling from A-MWCNT exposure, and interleukin-1 signaling from uncoated-MWCNT exposure. These studies provide key insight into the mechanisms of cellular response upon *in vitro* exposure to functionalized MWCNT.

Materials and Methods

CMRL cell medium 1066-1x, fungizone antimycotic (Fz), fetal bovine serum (FBS), glutamine, penicillin-streptomycin, Trump's transmission electron microscopy (TEM) fixative, noble agar, and the pierce lactate dehydrogenase (LDH) assay kit were purchased from ThermoFisher Scientific (Waltham, MA). Acetic acid, ammonium bicarbonate, sodium deoxycholate (SDC), dithiothreitol (DTT), iodoacetamide (IAM), formic acid (FA),

Author Manuscript Author Manuscript Author Manuscript Author Manuscript

ammonium hydroxide, hydrochloric acid (HCl), and bovine serum albumin (BSA) were obtained from Sigma Aldrich (St. Louis, MO). Diethylzinc (DEZ) and trimethylaluminum (TMA) were purchased through Strem Chemicals at a minimum 98% purity (Newburyport, MA). Multi-walled carbon nanotubes (MWCNTs) were purchased at Helix Materials Solutions, Inc. (Richardson, TX) at 0.5–40 μm in length. P-type (<100>) silicon substrates were acquired through University Wafers (Boston, MA). High purity nitrogen gas was purchased from Machine & Welding Supply Co. Sequencing grade trypsin was purchased from Promega (Madison, WI). HPLC grade water, methanol, and acetonitrile were purchased from VWR International (Morrisville, NC). Oasis MCX 30 μm particle size solid phase extraction cartridges were obtained from Waters (Milford, MA).

Nanomaterials

MWCNTs 0.5 – 40 μm in length were synthesized by chemical vapor deposition. Characterization of the MWCNTs was provided by the manufacturer and verified by Millennium Research Laboratories (Woburn, MA) [21]. Some of the MWCNTs were coated with conformal nanoscale thin films of aluminum oxide or zinc oxide by atomic layer deposition (ALD) (Figure 1). Zinc oxide coating was achieved by co-reacting DEZ and deionized (DI) water. The aluminum oxide layer was achieved using sequential saturated exposures of TMA ($Al(CH_3)_3$) and water. Both reactions were conducted in a custom made, viscous-flow, hot-walled, vacuum reactor and purged with high purity nitrogen gas, and then further purified with an Entegris GateKeeper upstream from the reactor input [22–24]. TEM and mass gain were used to monitor the growth rate for the aluminum oxide and zinc oxide ALD coating process on MWCNTs; both types of nanotubes used in this study had a coating of roughly 10 nm. The details of ALD coating of carbon nanotubes have been previously described [17, 25, 16].

Preparation of MWCNTs

Uncoated MWCNTs (U-MWCNT), aluminum oxide coated (A-MWCNT), and zinc oxide coated (Z-MWCNT) were weighed using a milligram scale (Mettler, Toledo OH) suspended in a sterile 0.1% pluronic F-68 (Sigma-Aldrich, St. Louis MO) phosphate buffer solution to achieve the final concentration of 10 mg/mL. Vials containing the suspended nanomaterials were dispersed using a cuphorn sonicator (Qsonica, Newton CT) at room temperature for 1 minute prior to dosing. The A-MWCNT and Z-MWCNT concentrations were normalized to the U-MWCNT nanoparticle number in order to account for the mass increase caused by the surface modification of the CNT. The A-MWCNT were dosed at 2.5 times the U-MWCNT dose and the Z-MWCNT were dosed at 2.85 times the U-MWCNT dose. A limulus amebocyte lysate chromogenic assay (Lonza Inc., Walkersville MD) was used to test the nanomaterials for endotoxin contamination. All MWCNTs tested negative (< 0.3 EU/mL) for endotoxin.

Dynamic Light Scattering Analyses

U-MWCNT, A-MWCNT and Z-MWCNT suspensions were made as described in the preparations of MWCNTs section. Hydrodynamic diameter, size distribution and zeta potential of the freshly prepared suspensions in E10 cell culture media (Supplemental Method- Cell Culture) were determined using dynamic light scattering (ZetaSizer Nano,

Author Manuscript Author Manuscript Author Manuscript Author Manuscript

Malvern Instruments, Westborough, MA) as described previously [26]. Electrophoretic mobility was converted into zeta potential using the Helmholtz-Smoluchowski equation (Supplemental Table 1).

Cell Culture

E10 alveolar epithelial cells were provided as a kind gift from Dr. Michael Fessler at the National Institute of Environmental Health Sciences (NIEHS) and were originally derived from the laboratory of Dr. Joseph Mizgerd at Boston University School of Medicine [20]. The E10 cell culture was maintained as described in Supplemental Method- **Cell Culture**.

Experimental Design

A Latin square block design was used for the experimental setup of the MWCNT E10 cell dosing in order to control for plate affect, thus reducing experimental bias (Figure 2). Every treatment (i.e. dose) was assigned a random number using a random number generator, and was then dosed accordingly as a Latin square design. Each dose and coating type had 4 replicates to account for biological variability; also known as biological replicates. 6-well plates contained 2 control wells (no MWCNT exposure) and 4 treatments wells (MWCNT exposure) [27]. A total of 36 cell culture samples were collected, 1 of the samples was randomly picked and was digested twice to generate technical replicates, and 10 samples were run as analytical replicates on the orbitrap LC-MS/MS (48 injections total). A detailed description of the cellular MWCNT exposure and isolation can be found in Supplemental Method- Exposure and Isolation.

Cytotoxicity Assay

An LDH assay was conducted to evaluate cytotoxicity in order to ensure appropriate dose concentration by coating type [28]. The E10 cells were exposed to U-, A-, and Z-MWCNT in the following concentrations to establish a dose response curve: 0, 5, 10, 25, 50, 100 μg/mL (see above sections for how MWCNT were prepared for dosing). The LDH assay was conducted on 50 μL samples of media from MWCNT cell culture exposure with 2 replicates per sample. Absorbance was measured using a multiskan^{TM} microplate photometer (ThermoFisher), and the percent cytotoxicity was calculated by the manufacture's protocol.

Protein Digestion and LC-MS/MS

Details regarding the in solution protein digestion are provided in Supplemental Methods- Protein Digestion. Nanoflow liquid chromatography (LC) was conducted using the Thermo Scientific Easy-nLC 1000 Liquid Chromatography system. Details regarding all LC methods can be found in Supplemental Method- Nanoflow LC (Supplemental Table 2). Methods for global tandem mass spectrometry (MS) data collection using a dependent acquisition mode (DDA), and targeted MS data collected using a selected reaction monitoring (SRM) are thoroughly described in Supplemental Method- Mass Spectrometry.

Author Manuscript Author Manuscript Author Manuscript Author Manuscript

Database Search

Database searches were conducted using Proteome Discoverer 1.4 and the Sequest hyper-threaded algorithm. Data were searched against the *Mus Musculus* Swiss Prot protein database (number of sequences: 16657, date accessed: 06/30/2015) [29]. Peptide spectrum matches were post processed using percolator [30] to enforce a peptide spectral match threshold of less than 0.01 q value, the minimal false discovery threshold to which a spectral identification is accepted as correct. The law of strict parsimony was used for protein inference and grouping [31].

Data Analysis

Peak area data generated from Proteome Discoverer label free node was exported as a text file, and further analyzed using R version 3.2.2. Protein peak area was first $\log_{10}$ transformed and plotted as box-and-whisker plots to ensure all samples maintained roughly the same minimum, median, and maximum peak area values (Supplemental Figure 1). In order to remove proteins that generated inconsistent results, the data were filtered by retaining proteins that had detection in at least 3 out of 4 biological replicates (i.e. protein maintained signal in 75% of the biological replicates within control or exposure groups). Additionally, proteins were retained if they did not have signal across all biological replicates in one group (i.e. all of the A-MWCNT 100 μg/mL dosed samples did not have expression for protein x, but all of the U-MWCNT 100 μg/mL dosed samples had expression for protein x). Thus, proteins were removed from the protein list if peak area signal was inconsistent within a class of samples. Data were then central tendency median normalized, followed by imputation of missing values with the minimum peak area across entire data set [32]. Principal component analysis (PCA) was used to screen for potential confounding effects; such as plate effects. A two-sample Welch t-test was conducted by pairwise comparison of protein peak area across each exposure compared to control. Analysis of variance (ANOVA) was conducted using **equation 1**, and results can be found in Supplemental Method- ANOVA. Ingenuity pathway analysis was used for enrichment analysis [33]. Targeted peak area data was examined and exported from skyline-daily for further analysis.

Equation 1
Analysis of variance model of peak area for proteins in common across each coating type.

$$\text{Peak Area} = \text{Intercept} + \text{Dose} + \text{Coating}$$

Orbitrap LC-MS/MS

The E10 data set contained 48 LC-MS/MS runs, including: biological, technical, and analytical replicates. An average of 2200 protein groups were identified by LC-MS/MS in DDA mode. After filtering, normalizing, and imputing (as described in the data analysis section), 1576 proteins were retained for further expression analysis.

Author Manuscript Author Manuscript Author Manuscript Author Manuscript

Triple Quadrupole LC-MS/MS

While DDA is a powerful method to assess global proteomics, the nature of the method yields the potential for incomplete sampling of peptides [34], thus verification of relative protein abundance is ideal for confirming accurate quantitation. We verified differential protein abundance from the discovery proteomics experiment using a triple quadrupole mass spectrometer operating in selected reaction monitoring (SRM) mode. Proteins were screened for the verification to represent high and low abundance. A single unique peptide was chosen as a proxy for protein abundance and the method was exported using Skyline. Raw data were imported into the created Skyline template and each individual peptide was manually evaluated to ensure retention time reproducibility, high dot product (>0.8, match between discovery and targeted data), and proper integration boundaries. A pairwise comparison of peptide abundance for each MWCNT exposure versus control (i.e. A-MWCNT versus control) was conducted in order to represent expression fold change for validation of the DDA data with targeted SRM data (Supplemental Figure 2). A Pearson's correlation coefficient indicated the discovery differential proteomics data strongly correlated with the targeted proteomics data ($r = 0.9635$) (Supplemental Table 3).

Results

Exposure Dose-Response

A general overview of the experimental design is illustrated in Figure 2. Dose-response curves were generated for the E10 cell line by exposing cells to the following doses of U-MWCNT, A-MWCNT, and Z-MWCNT: 0, 1, 5, 10, 50, and 100 (μg/mL) (Figure 3). Both U-MWCNT and A-MWCNT showed no cytotoxicity according to the LDH assay; however, the Z-MWCNT showed 100% cytotoxicity at the 10 μg/mL dose. The dose-response results were used to set a 'low' and 'high' exposure range for the dosing of E10 cells. The following doses were given in biological replicates of 4: U-MWCNT dosed at 5 and 100 μg/mL, A-MWCNT dosed at 5 and 100 μg/mL, and Z-MWCNT was dosed at 2.5 and 5 μg/mL (lower dose of Z-MWCNT to adjust for cytotoxicity).

Characterization of MWCNTs in Cell Culture Media

Dry U-MWCNTs have been previously characterized in terms of length, width, residual metals and agglomeration status [21]. U-MWCNTs are 30 to 50 nm in diameter and have a heterogeneous range of 0.3 to 50 micrometers in length, and a surface area of 40 to 300 m^2/g. A-MWCNTs and Z-MWCNTs produced by ALD coating of U-MWCNTs have also been thoroughly characterized width, length, and thickness of metal oxide coating and the details of these ALD-functionalized tubes are previously published [16, 17].

We also sought to characterize these nanomaterials after addition to the cell culture media used for maintaining E10 cells. Specifically, we measured hydrodynamic diameter as an indication of MWCNT agglomeration size in media and zeta potential as an index of surface charge (Supplemental Table 1). A-MWCNTs and Z-MWCNTs had reduced hydrodynamic diameters (416 nm and 192 nm respectively) compared to U-MWCNTs (567 nm), indicating less agglomeration and better dispersion. A-MWCNTs and Z-MWCNTs did not have

Author Manuscript Author Manuscript Author Manuscript Author Manuscript

significantly different zeta potential or polydispersity indices, indicating that the ALD coatings applied to MWCNTs did not alter surface charge.

TEM Imaging

TEM images of the E10 cells dosed in this experiment clearly show each type of MWCNT were taken up by the alveolar epithelial cells (Figure 4 A–C). The Al_2O_3 coating on A-MWCNTs remained intact after cellular uptake (Figure 4 B). Interestingly, U-MWCNT were similar to Z-MWCNT in appearance after uptake by epithelial cells (Figure 4 A and 4 C respectively), indicating that the Z-MWCNT coating was lost. Our previous work demonstrated that Zn^{+2} ions are released after Z-MWCNTs are added to cell culture media, indicating at least partial dissolution of the ALD coating [17]. Other studies have indicated that partial dissolution of ZnO nanoparticles occurs in the cell media but complete dissolution of the nanoparticles likely occurs within the cell [35, 36]. Methods used for TEM preparation can be found in Supplemental Methods- TEM imaging.

E10 Proteomic Expression Changes

Of the 1576 proteins retained for global expression analysis, the following number of proteins were found to be significant by t-test ($p < 0.05$) at the highest dose of each exposure (i.e. 100 μg/mL for U- and A-MWCNT, and 5 μg/mL Z-MWCNT): 138 U-MWCNT versus control, 210 A-MWCNT versus control, 103 Z-MWCNT versus control (Supplemental Table 4). Fewer proteins were found to be significant in each ‘low’ dose exposure, and results can be found in Supplemental Table 5. Due to the limited significance found in the low dose exposure, the results will not be discussed herein. Further analysis was conducted on the ‘high’ dose exposure to evaluate if the same proteins shared significance across each exposure type versus control to possibly indicate shared cellular response mechanisms. Interestingly, Venn diagrams plotted by categories of ‘increased’ and ‘decreased’ regulation of significantly differentially expressed proteins by t-test show little overlap in commonly significant proteins (Figure 5). Common proteins found for increased expression by exposure compared to control include: hemoglobin subunit beta, hemoglobin subunit gamma, and proteolipid protein 2. The common protein found for the decreased expression is fatty acid synthase.

Pathway Analysis

Pathway analysis was conducted using ingenuity pathway analysis (IPA) on the significant proteins for each MWCNT exposure compared to control. First, all of the significantly differentially expressed proteins, separated by increased or decreased expression relative to the control, were imported into IPA one MWCNT exposure group at a time. Pathways for each MWCNT exposure were generated in IPA using the core analysis search, and the search species was specified as mouse. Comparison analyses were then conducted on each set of enriched pathways for exposure compared to control. Results shown in Figure 6 illustrate heat maps generated in R using the data output from IPA to compare pathways with increased pathway enrichment (Figure 6 A), and suppressed pathway enrichment (Figure 6 B) for exposure relative to control. The heat maps were re-created in R by transforming the $-\log_{10} p$ value output from IPA into Z scores, with dark red being the most significant p value and dark blue being the least significant. Supplemental Table 6 lists the $-\log_{10} p$ value

Author Manuscript Author Manuscript Author Manuscript Author Manuscript

associated with each pathway across every MWCNT exposure. While several pathways exhibit significant differential protein expression, the following pathways will be discussed herein to better highlight the unique proteomic responses as a function of MWCNT coating type: inhibition of angiogenesis by thrombospondin-1, mTOR/eIF4/p70S6K signaling, oxidative phosphorylation, interleukin-1 signaling, and Nrf-2 mediated oxidative stress response. Furthermore, the protein peak area $\log_2$ fold change associated with each exposure versus control were plotted as heat maps to illustrate specific changes in protein expression related to pathways of interest (Figure 7, Supplemental Table 7).

Discussion

The aim of this study was to investigate how the alveolar epithelial cell proteome might be influenced by exposure to different MWCNT ALD coating types through a shotgun proteomics approach. Differential expression patterns obtained in cell culture can identify mechanisms of cellular response, which may help to predict toxicity and biological outcome in the lungs of mice and humans. To better understand mechanisms of the alveolar epithelial cell response to MWCNT *in vitro* exposures, pathway analysis was used to map cellular function to statistically differentially expressed proteins. Results from the pathway analysis demonstrate that either aluminum oxide-coated MWCNT (A-MWCNT) or zinc oxide-coated MWCNT (Z-MWCNT) had both common and unique pathway enrichment that represents significant differences in cellular response compared to uncoated MWCNT (U-MWCNT) exposure. The following pathway enrichments will be discussed in further detail: Nrf-2 mediated oxidative stress response, interleukin-1 signaling, inhibition of angiogenesis by thrombospondin-1, mTOR/eIF4/p70S6K signaling, and oxidative phosphorylation.

Nrf-2 Mediated Oxidative Stress Response

The nuclear factor erythroid 2-related factor 2 (Nrf2)- mediated oxidative stress response pathway has been established as a significant survival response upon exposure to various environmental toxicants that are known to cause oxidative stress [37]. More specifically, the activation of the Nrf2 signaling pathway is inversely proportional to inflammatory and pro-fibrotic cytokines. Studies have shown the importance of Nrf2 activation by exposing Nrf2 knockout mice to MWCNTs, which yielded excessive oxidative stress relative to the control exposure [38]. Of the exposures given in this study, Z-MWCNT had the most significant enrichment for the Nrf2 mediated oxidative stress response relative to control with 8 proteins showing significant increased enrichment relative to control (pathway enrichment p-value = 2.80E-07).

Our previous investigation revealed that Z-MWCNT exposure to THP-1 cells *in vitro* stimulate pro-inflammatory cytokine expression [17]. This pro-inflammatory pulmonary stress response has been routinely quantified by measuring antioxidant gene expression, such as heme oxygenase 1 (HO-1), and other proteins downstream of Nrf2 signaling (Figure 7 A) [39]. Interestingly, zinc oxide was the only MWCNT coating to cause a significant increase in HO-1 (p-value = 0.001), thus indicating that the Z-MWCNT exposure is causing an oxidative stress response leading to Nrf2 activation and significantly increased HO-1 expression.

Author Manuscript Author Manuscript Author Manuscript Author Manuscript

Interleukin-1 Signaling Pathway

The interleukin-1 (IL-1) family is a group of 11 cytokines which are known to mediate inflammatory response [40]. Activation of the IL-1 signaling pathway occurs as a stress response in order to produce various pro-inflammatory mediators [41]. Several studies have shown that MWCNT exposure causes acute inflammation via inflammasome activation and release of IL-1β that binds to specific receptors on a variety of lung cells to mediate acute inflammation [42–44, 26]. While the IL-1 proteins were not detected in this study due to potential limitation in dynamic range, downstream proteins showed enrichment for IL-1 signaling activation. Significant enrichment of 5 proteins downstream of the IL-1 signaling pathway were found in the U-MWCNT exposure (pathway enrichment *p*-value = 1.620E-06). Of the proteins enriched through the U-MWCNT exposure for IL-1 signaling pathway, mitogen-activated protein kinase 14 (MAPK14) is perhaps the most critical protein due to its essential role in inflammatory cytokine induction (Figure 7 B) [45]. MAPK14 was significantly upregulated in the U-MWCNT exposure (*p*-value = 0.043), but not the coated exposures to A- or Z-MWCNT, thus indicating that the alveolar epithelial cells present a stronger downstream IL-1 signaling response to U-MWCNT exposure.

Inhibition of Angiogenesis by Thombospondin-1

Angiogenesis, the process by which new blood vessels are formed, plays an integral role in the regulation of promotors that contribute to pulmonary hypertension and pulmonary fibrosis [46]. The regulation of angiogenesis is primarily controlled by fibroblast growth factor (FGF), vascular endothelial growth factor (VEGF), and heparan sulfate proteoglycans (HSPG) proteins [47]. HSPGs can act to inhibit angiogenesis through signaling from thrombospondin-1 (TSP-1) [48]. TSP-1 is a matricellular glycoprotein that plays an influential role in the structure of cellular matrix, and can have direct and indirect inhibition of angiogenesis. The direct effects on inhibition occur via TSP-1 signaling to HSPG which inhibit angiogenesis, and indirect effects by TSP-1 binding to and activating transforming growth factor beta (TGF-beta) [49].

In addition to significant contributions to angiogenesis and pulmonary hypertension, TSP-1 has been reported to have increased expression in malignant mesotheliomas caused by asbestos exposure [50], thus suggesting MWCNT exposure may induce a similar mechanism of cellular response as exposure to asbestos due to similarities in physical properties. The results from this *in vitro* study show that TSP-1 was significantly upregulated in A-MWCNT (*p*-value = 2.53E-05) and U-MWCNT (*p*-value = 0.003) exposures (Figure 7 C). The following proteins were significantly increased in expression upon A-MWCNT exposure and enriched for in the inhibition of angiogenesis signaling pathway: TSP-1 and tyrosin-protein kinase fyn (FYN). Additionally, U-MWCNT exposure drove significant upregulation in TSP-1, FYN, and MAPK14. Ultimately, the A- and U-MWCNT exposures generated significant proteins that were enriched in the inhibition of angiogenesis pathway, thus indicating their contributions to inhibit angiogenesis.

mTOR/eIF4/p70S6K Signaling Pathway

Signaling from mammalian targeting of rapamycin (mTOR), like angiogenesis, has been reported to play a critical role in vascular remodeling and has been implicated for its

Author Manuscript Author Manuscript Author Manuscript Author Manuscript

contributions to pulmonary disease through the progression of pulmonary hypertension [51]. mTOR signaling can be induced by growth factors, and has also been well established for its contribution to regulating autophagy [52]. Under cellular stress and limited energy, mTOR signaling is repressed and autophagic signaling can be initiated [53]. Additional mediators of autophagy that are regulated by mTOR signaling include p70S6k and eIF4 proteins, which are reported to lead to translation of proteins that mediate cell cycle activators, ribosome biogenesis, and angiogenesis [54]. The results from this study show mTOR/eIF4/p70S6K signaling pathways have significant enrichment upon Z-MWCNT exposure (p-value = 1.46E-09 mTOR signaling, and p-value = 5.59124E-08 eIF4/p70S6K signaling), but not A- and U-MWCNT exposure (Figure 7 D and 7 E). Moreover, 10 proteins are significantly upregulated in the Z-MWCNT exposure that are downstream of the mTOR/eIF4/p70S6K signaling pathway, thus indicating activation of signaling by Z-MWCNT compared to control. These results suggest that the Z-MWCNT drive increased expression of protein mediators that contribute to cell proliferation that were not significant in the U-MWCNT and A-MWCNT exposures.

Oxidative phosphorylation

Oxidative phosphorylation (OXPHOS) is the metabolic pathway comprised of protein complexes that make up the mitochondrial electron transport chain, and function to generate ATP [55]. OXPHOS signaling is generally associated with mitochondrial function and ultimately effect the oxidative state of the cell, which can serve a critical marker for injury. Several pathways can be initiated in response to a change in oxidative state in the cell, including cell survival or cell death via apoptosis or necrosis [56]. More specifically, there is a sensitive intracellular balance in response to oxidative stress between mitochondrial biogenesis and mitochondrial dysfunction [57]. Several studies have shown mitochondrial dysfunction as a result of excessive oxidative stress during hyperoxia [58], as well as asbestos exposure [59] and MWCNT exposure [60].

The most significant increased enrichment for the OXPHOS signaling response was found in the A-MWCNT (pathway enrichment p-value = 4.26E-10). Proteins associated with the mitochondrial dysfunction pathway were also significantly enriched for in the A-MWCNT exposure (p-value = 8.50E-11). Of the 14 proteins enriched for mitochondrial dysfunction, 11 were increased in A-MWCNT exposure, and 5 proteins were increased for U-MWCNT (Figure 7 F). Most of the upregulated proteins enriched across both exposures were identified as proteins in the electron transport chain. Overall, the increased expression for the proteins enriched in OXPHOS and mitochondrial dysfunction pathways associated with aluminum oxide coated and uncoated MWCNT exposure may indicate metabolic adaptation to help counter the pro-fibrogenic effect of MWCNT exposure observed *in vivo* and *in vitro* [16].

Common Protein Expression

While most of the proteins upregulated upon exposure to ALD coated and uncoated MWCNT produced differential expression related to different pathways, one protein showed significant upregulation across every exposure relative to control: Hemoglobin (Hb). Alveolar Type II epithelial cells have been reported to express Hb in several cell lines, both

Author Manuscript Author Manuscript Author Manuscript Author Manuscript

primary and transformed [61]. There have also been studies reporting increased Hb expression in response to oxidative stress, thus implicating the pulmonary epithelium may play a role in protection against oxidative/nitrosative stress [62, 63]. Both coated and uncoated MWCNT exposure exhibited increased beta-Hb and gamma-Hb expression compared to the corresponding Hb subunit levels expressed in the control samples (Supplemental Table 4). Note, the alpha-Hb sub-unit was also highly expressed in each MWCNT exposure, but that protein was removed during data filtering due to variable low expression in the control samples. Therefore, a common protective mechanism in response to MWCNT exposure may be through increased Hb expression in order to scavenge free oxygen and nitric oxide species.

In vitro versus In vivo Comparison

The proteomic results from the E10 mouse alveolar epithelial cells *in vitro* revealed mechanisms of cellular response that were not characterized in our previous mouse *in vivo* studies using the same ALD coated MWCNTs [17, 16]. For example, mice exposed to A-MWCNTs by oropharyngeal aspiration had elevated levels of IL-1β in BALF compared to animals treated with U-MWCNTs [16]. Mice exposed to Z-MWCNTs by oropharyngeal aspiration exhibited high levels of the acute phase reactant protein IL-6 in BALF [17]. However, the endpoints for both of the previous studies were limited to only a few selected cytokines that were measured by ELISA and did not yield a strong bases for comparison for proteomic results. Also, the cytokines measured in the previous *in vivo* studies could have been produced by cell types other than alveolar epithelial cells such as alveolar macrophages or fibroblasts. Finally, our results in the present study with E10 cells focused only on intracellular proteins since evaluation of secreted proteins would have been confounded by serum proteins present in the cell culture medium. Therefore, there are some limitations of *in vitro* cell culture experiments for predicting disease outcomes *in vivo*. Nonetheless, the results of the proteomic analysis of E10 cells in the present study is an important step towards identifying new molecular targets and biomarkers of disease that can be further investigated in future mouse exposure studies.

Conclusion

Given that CNT functionalization will yield a diversity of nanomaterials that have unknown potential to cause pulmonary diseases, more sensitive and high-throughput toxicity screening needs be developed to raise awareness of unique nanomaterial hazards. Markers for toxicity can be found in differential protein response as a function of CNT coating type. Tools like pathway enrichment can be used to aid the screening process by mapping statistically significant differentially expressed proteins to a biological function. Unique pathway regulation was found in this study through the following results: increased autophagy signaling from Z-MWCNT exposure, increased mitochondrial dysfunction and oxidative phosphorylation from A-MWCNT exposure, and increased interluekin-1 signaling from U-MWCNT exposure. Ultimately, this study demonstrates the use of proteomics as a powerful sensitive measurement technique that can unravel differential cellular protein expression in cultured lung epithelial cells as a function of CNT coating type. Moreover,

Author Manuscript Author Manuscript Author Manuscript Author Manuscript

these differential cellular protein expression profiles may be useful towards screening carbon nanotubes for toxicity and predicting hazard for human exposure.

Supplementary Material

Refer to Web version on PubMed Central for supplementary material.

Acknowledgments

The authors acknowledge support from the National Institute of Environmental Health Sciences (NIEHS) Training Grant: T32 ES007046 (GSH), NIEHS R01ES020897 (JCB, GNP, ECD, AJT), and NIEHS P30ES025128 (MSB, GSH, EHG). This work was also supported (in part) by the NIEHS Intramural Research Program (SH, SG)

List of abbreviations

Al_2O_3	Aluminum oxide
A-MWCNT	Aluminum oxide-coated multi-walled carbon nanotubes
ALD	Atomic layer deposition
CNTs	Carbon nanotubes
DDA	Data dependent acquisition
HPLC	High-performance liquid chromatography
IT	Intratracheal instillation
IPA	Ingenuity Pathway Analysis
LC-MS/MS	Liquid chromatography tandem mass spectrometry
MWCNT	Multi-walled carbon nanotubes
NIEHS	National Institute of Environmental Health Sciences
PTMs	Post-translational modifications
PCA	Principal component analysis
SRM	Selected reaction monitoring
SWCNT	Single-walled carbon nanotubes
U-MWCNT	Un-coated multi-walled carbon nanotubes
Z-MWCNT	Zinc oxide-coated multi-walled carbon nanotubes

References

1. Donaldson K, Aitken R, Tran L, Stone V, Duffin R, Forrest G, et al. Carbon nanotubes: a review of their properties in relation to pulmonary toxicology and workplace safety. Toxicological sciences : an official journal of the Society of Toxicology. 2006; 92(1):5–22. DOI: 10.1093/toxsci/kfj130 [PubMed: 16484287]

Author Manuscript Author Manuscript Author Manuscript Author Manuscript

2. Eatemadi A, Daraee H, Karimkhanloo H, Kouhi M, Zarghami N, Akbarzadeh A, et al. Carbon nanotubes: properties, synthesis, purification, and medical applications. Nanoscale research letters. 2014; 9(1):393.doi: 10.1186/1556-276X-9-393 [PubMed: 25170330]
3. Prato M, Kostarelos K, Bianco A. Functionalized carbon nanotubes in drug design and discovery. Accounts of chemical research. 2008; 41(1):60–8. DOI: 10.1021/ar700089b [PubMed: 17867649]
4. Singh S, Kruse P. Carbon nanotube surface science. International Journal of Nanotechnology. 2008; 5(9/10/11/12):900.doi: 10.1504/ijnt.2008.019826
5. Hyde GK, McCullen SD, Jeon S, Stewart SM, Jeon H, Loboa EG, et al. Atomic layer deposition and biocompatibility of titanium nitride nano-coatings on cellulose fiber substrates. Biomedical materials. 2009; 4(2):025001.doi: 10.1088/1748-6041/4/2/025001 [PubMed: 19208941]
6. Peng Q, Sun XY, Spagnola JC, Hyde GK, Spontak RJ, Parsons GN. Atomic layer deposition on electrospun polymer fibers as a direct route to AL2O3 microtubes with precise wall thickness control. Nano letters. 2007; 7(3):719–22. DOI: 10.1021/nl062948i [PubMed: 17279801]
7. Parsons GN, George SM, Knez M. Progress and future directions for atomic layer deposition and ALD-based chemistry. MRS Bulletin. 2011; 36(11):865–71. DOI: 10.1557/mrs.2011.238
8. Poland CA, Duffin R, Kinloch I, Maynard A, Wallace WA, Seaton A, et al. Carbon nanotubes introduced into the abdominal cavity of mice show asbestos-like pathogenicity in a pilot study. Nature nanotechnology. 2008; 3(7):423–8. DOI: 10.1038/nnano.2008.111
9. WHO. Asbestos. World Health Organization; 2015. http://www.who.int/ipcs/assessment/public_health/asbestos/en/ [Accessed 12/18/2015 2015]
10. Madani SY, Mandel A, Seifalian AM. A concise review of carbon nanotube's toxicology. Nano reviews. 2013; :4.doi: 10.3402/nano.v4i0.21521
11. NIH. [Accessed 11/20/2014] What Is Idiopathic Pulmonary Fibrosis?. 2011. http://www.nhlbi.nih.gov/health/health-topics/topics/ipf/
12. Mercer RR, Hubbs AF, Scabilloni JF, Wang L, Battelli LA, Friend S, et al. Pulmonary fibrotic response to aspiration of multi-walled carbon nanotubes. Particle and fibre toxicology. 2011; 8:21.doi: 10.1186/1743-8977-8-21 [PubMed: 21781304]
13. Cheresh P, Kim SJ, Tulasiram S, Kamp DW. Oxidative stress and pulmonary fibrosis. Biochimica et biophysica acta. 2013; 1832(7):1028–40. DOI: 10.1016/j.bbadis.2012.11.021 [PubMed: 23219955]
14. He X, Young SH, Schwegler-Berry D, Chisholm WP, Fernback JE, Ma Q. Multiwalled carbon nanotubes induce a fibrogenic response by stimulating reactive oxygen species production, activating NF-kappaB signaling, and promoting fibroblast-to-myofibroblast transformation. Chemical research in toxicology. 2011; 24(12):2237–48. DOI: 10.1021/tx200351d [PubMed: 22081859]
15. Bonner JC. Nanoparticles as a potential cause of pleural and interstitial lung disease. Proceedings of the American Thoracic Society. 2010; 7(2):138–41. DOI: 10.1513/pats.200907-061RM [PubMed: 20427587]
16. Taylor AJ, McClure CD, Shipkowski KA, Thompson EA, Hussain S, Garantziotis S, et al. Atomic layer deposition coating of carbon nanotubes with aluminum oxide alters pro-fibrogenic cytokine expression by human mononuclear phagocytes in vitro and reduces lung fibrosis in mice in vivo. PloS one. 2014; 9(9):e106870.doi: 10.1371/journal.pone.0106870 [PubMed: 25216247]
17. Dandley EC, Taylor AJ, Duke KS, Ihrie MD, Shipkowski KA, Parsons GN, et al. Atomic layer deposition coating of carbon nanotubes with zinc oxide causes acute phase immune responses in human monocytes in vitro and in mice after pulmonary exposure. Particle and fibre toxicology. 2016; 13(1)doi: 10.1186/s12989-016-0141-9
18. Costa PM, Fadeel B. Emerging systems biology approaches in nanotoxicology: Towards a mechanism-based understanding of nanomaterial hazard and risk. Toxicology and applied pharmacology. 2015; doi: 10.1016/j.taap.2015.12.014
19. Schmidt A, Forne I, Imhof A. Bioinformatic analysis of proteomics data. BMC systems biology. 2014; 8(Suppl 2):S3.doi: 10.1186/1752-0509-8-S2-S3
20. Yamamoto K, Ferrari JD, Cao Y, Ramirez MI, Jones MR, Quinton LJ, et al. Type I alveolar epithelial cells mount innate immune responses during pneumococcal pneumonia. Journal of immunology. 2012; 189(5):2450–9. DOI: 10.4049/jimmunol.1200634

Author Manuscript Author Manuscript Author Manuscript Author Manuscript

21. Ryman-Rasmussen JP, Tewksbury EW, Moss OR, Cesta MF, Wong BA, Bonner JC. Inhaled multiwalled carbon nanotubes potentiate airway fibrosis in murine allergic asthma. American journal of respiratory cell and molecular biology. 2009; 40(3):349–58. DOI: 10.1165/rcmb.2008-0276OC [PubMed: 18787175]
22. Gong B, Peng Q, Jur JS, Devine CK, Lee K, Parsons GN. Sequential Vapor Infiltration of Metal Oxides into Sacrificial Polyester Fibers: Shape Replication and Controlled Porosity of Microporous/Mesoporous Oxide Monoliths. Chemistry of Materials. 2011; 23(15):3476–85. DOI: 10.1021/cm200694w
23. Jur JS, Spagnola JC, Lee K, Gong B, Peng Q, Parsons GN. Temperature-dependent subsurface growth during atomic layer deposition on polypropylene and cellulose fibers. Langmuir : the ACS journal of surfaces and colloids. 2010; 26(11):8239–44. DOI: 10.1021/la904604z [PubMed: 20163129]
24. Spagnola JC, Gong B, Arvidson SA, Jur JS, Khan SA, Parsons GN. Surface and sub-surface reactions during low temperature aluminium oxide atomic layer deposition on fiber-forming polymers. Journal of Materials Chemistry. 2010; 20(20):4213.doi: 10.1039/c0jm00355g
25. Devine CK, Oldham CJ, Jur JS, Gong B, Parsons GN. Fiber containment for improved laboratory handling and uniform nanocoating of milligram quantities of carbon nanotubes by atomic layer deposition. Langmuir : the ACS journal of surfaces and colloids. 2011; 27(23):14497–507. DOI: 10.1021/la202677u [PubMed: 22070742]
26. Hussain S, Sangtian S, Anderson SM, Snyder RJ, Marshburn JD, Rice AB, et al. Inflammasome activation in airway epithelial cells after multi-walled carbon nanotube exposure mediates a profibrotic response in lung fibroblasts. Particle and fibre toxicology. 2014; 11:28.doi: 10.1186/1743-8977-11-28 [PubMed: 24915862]
27. Gumpertz, FGGaML. Planning, Construction, and Statistical Analysis of Comparative Experiments. John Wiley & Sons; 2004.
28. Scientific, T. [Accessed 09/30/2015 2015] Pierce LDH Cytotoxicity Assay Kit. 2015. https://www.thermofisher.com/order/catalog/product/88953
29. Bairoch A. The SWISS-PROT protein sequence data bank and its new supplement TREMBL. Nucleic acids research. 1996; 24(1):21–5. DOI: 10.1093/nar/24.1.21 [PubMed: 8594581]
30. Kall L, Canterbury JD, Weston J, Noble WS, MacCoss MJ. Semi-supervised learning for peptide identification from shotgun proteomics datasets. Nature methods. 2007; 4(11):923–5. DOI: 10.1038/nmeth1113 [PubMed: 17952086]
31. Zhang B, Chambers MC, Tabb DL. Proteomic parsimony through bipartite graph analysis improves accuracy and transparency. Journal of proteome research. 2007; 6(9):3549–57. DOI: 10.1021/pr070230d [PubMed: 17676885]
32. Karpievitch YV, Dabney AR, Smith RD. Normalization and missing value imputation for label-free LC-MS analysis. BMC bioinformatics. 2012; 13(Suppl 16):S5.doi: 10.1186/1471-2105-13-S16-S5
33. IPA. Ingenutiry Pathway Analysis. QIAGEN; 2016. www.qiagen.com/ingenuity [Accessed 05/05/2016 2016]
34. Michalski A, Cox J, Mann M. More than 100,000 detectable peptide species elute in single shotgun proteomics runs but the majority is inaccessible to data-dependent LC-MS/MS. Journal of proteome research. 2011; 10(4):1785–93. DOI: 10.1021/pr101060v [PubMed: 21309581]
35. Gilbert B, Fakra SC, Xia T, Pokhrel S, Madler L, Nel AE. The fate of ZnO nanoparticles administered to human bronchial epithelial cells. ACS nano. 2012; 6(6):4921–30. DOI: 10.1021/nn300425a [PubMed: 22646753]
36. Xia T, Kovochich M, Liong M, Madler L, Gilbert B, Shi H, et al. Comparison of the mechanism of toxicity of zinc oxide and cerium oxide nanoparticles based on dissolution and oxidative stress properties. ACS nano. 2008; 2(10):2121–34. DOI: 10.1021/nn800511k [PubMed: 19206459]
37. Kensler TW, Wakabayashi N, Biswal S. Cell survival responses to environmental stresses via the Keap1-Nrf2-ARE pathway. Annual review of pharmacology and toxicology. 2007; 47:89–116. DOI: 10.1146/annurev.pharmtox.46.120604.141046
38. Dong J, Ma Q. Suppression of basal and carbon nanotube-induced oxidative stress, inflammation and fibrosis in mouse lungs by Nrf2. Nanotoxicology. 2015; :1–11. DOI: 10.3109/17435390.2015.1110758

Author Manuscript Author Manuscript Author Manuscript Author Manuscript

39. van Berlo D, Wilhelmi V, Boots AW, Hullmann M, Kuhlbusch TA, Bast A, et al. Apoptotic, inflammatory, and fibrogenic effects of two different types of multi-walled carbon nanotubes in mouse lung. Archives of toxicology. 2014; 88(9):1725–37. DOI: 10.1007/s00204-014-1220-z [PubMed: 24664304]
40. Dinarello CA. Interleukin-1 in the pathogenesis and treatment of inflammatory diseases. Blood. 2011; 117(14):3720–32. DOI: 10.1182/blood-2010-07-273417 [PubMed: 21304099]
41. Hirano S, Fujitani Y, Furuyama A, Kanno S. Uptake and cytotoxic effects of multi-walled carbon nanotubes in human bronchial epithelial cells. Toxicology and applied pharmacology. 2010; 249(1):8–15. DOI: 10.1016/j.taap.2010.08.019 [PubMed: 20800606]
42. Boyles M, Stoehr L, Schlinkert P, Himly M, Duschl A. The Significance and Insignificance of Carbon Nanotube-Induced Inflammation. Fibers. 2014; 2(1):45–74. DOI: 10.3390/fib2010045
43. Girtsman TA, Beamer CA, Wu N, Buford M, Holian A. IL-1R signalling is critical for regulation of multi-walled carbon nanotubes-induced acute lung inflammation in C57Bl/6 mice. Nanotoxicology. 2014; 8(1):17–27. DOI: 10.3109/17435390.2012.744110 [PubMed: 23094697]
44. Hamilton RF Jr, Buford M, Xiang C, Wu N, Holian A. NLRP3 inflammasome activation in murine alveolar macrophages and related lung pathology is associated with MWCNT nickel contamination. Inhalation toxicology. 2012; 24(14):995–1008. DOI: 10.3109/08958378.2012.745633 [PubMed: 23216160]
45. Han J, Lee J, Bibbs L, Ulevitch R. A MAP kinase targeted by endotoxin and hyperosmolarity in mammalian cells. Science. 1994; 265(5173):808–11. DOI: 10.1126/science.7914033 [PubMed: 7914033]
46. Smith JS, Gorbett D, Mueller J, Perez R, Daniels CJ. Pulmonary hypertension and idiopathic pulmonary fibrosis: a dastardly duo. The American journal of the medical sciences. 2013; 346(3): 221–5. DOI: 10.1097/MAJ.0b013e31827871dc [PubMed: 23313949]
47. Iozzo RV, San Antonio JD. Heparan sulfate proteoglycans: heavy hitters in the angiogenesis arena. The Journal of clinical investigation. 2001; 108(3):349–55. DOI: 10.1172/JCI13738 [PubMed: 11489925]
48. Lawler J. Thrombospondin-1 as an endogenous inhibitor of angiogenesis and tumor growth. Journal of Cellular and Molecular Medicine. 2002; 6(1):1–12. DOI: 10.1111/j.1582-4934.2002.tb00307.x [PubMed: 12003665]
49. Tirado-Rodriguez B, Ortega E, Segura-Medina P, Huerta-Yepez S. TGF- beta: an important mediator of allergic disease and a molecule with dual activity in cancer development. Journal of immunology research. 2014; 2014:318481.doi: 10.1155/2014/318481 [PubMed: 25110717]
50. Ohta Y, Shridhar V, Kalemkerian GP, Bright RK, Watanabe Y, Pass HI. Thrombospondin-1 expression and clinical implications in malignant pleural mesothelioma. Cancer. 1999; 85(12): 2570–6. DOI: 10.1002/(sici)1097-0142(19990615)85:12<2570::aid-cncr12>3.0.co;2-f [PubMed: 10375104]
51. Wang AP, Li XH, Yang YM, Li WQ, Zhang W, Hu CP, et al. A Critical Role of the mTOR/eIF2alpha Pathway in Hypoxia-Induced Pulmonary Hypertension. PloS one. 2015; 10(6):e0130806.doi: 10.1371/journal.pone.0130806 [PubMed: 26120832]
52. He C, Klionsky DJ. Regulation Mechanisms and Signaling Pathways of Autophagy. Annual Review of Genetics. 2009; 43(1):67–93. DOI: 10.1146/annurev-genet-102808-114910
53. Dunlop EA, Tee AR. mTOR and autophagy: a dynamic relationship governed by nutrients and energy. Seminars in cell & developmental biology. 2014; 36:121–9. DOI: 10.1016/j.semcdb.2014.08.006 [PubMed: 25158238]
54. Laplante M, Sabatini DM. mTOR signaling in growth control and disease. Cell. 2012; 149(2):274–93. DOI: 10.1016/j.cell.2012.03.017 [PubMed: 22500797]
55. Hatefi Y. The mitochondrial electron transport and oxidative phosphorylation system. Annual review of biochemistry. 1985; 54:1015–69. DOI: 10.1146/annurev.bi.54.070185.005055
56. Martindale JL, Holbrook NJ. Cellular response to oxidative stress: signaling for suicide and survival. Journal of cellular physiology. 2002; 192(1):1–15. DOI: 10.1002/jcp.10119 [PubMed: 12115731]
57. Suliman HB, Piantadosi CA. Mitochondrial Quality Control as a Therapeutic Target. Pharmacological reviews. 2016; 68(1):20–48. DOI: 10.1124/pr.115.011502 [PubMed: 26589414]

Author Manuscript Author Manuscript Author Manuscript Author Manuscript

58. Ratner V, Starkov A, Matsiukevich D, Polin RA, Ten VS. Mitochondrial dysfunction contributes to alveolar developmental arrest in hyperoxia-exposed mice. American journal of respiratory cell and molecular biology. 2009; 40(5):511–8. DOI: 10.1165/rcmb.2008-0341RC [PubMed: 19168698]

59. David, W., Kamp, VP., Weitzman, Sigmund A., Chandel, Navdeep. Asbestos-induced alveolar epithelial cell apoptosis: Role of mitochondrial dysfunction caused by iron-derived free radicals. In: Val Vallyathan, XSPD., Castranova, Vince, editors. Developments in Molecular and Cellular Biochemistry. Vol. 37. SpringerLink; 2002. p. 153-60.

60. Nymark P, Wijshoff P, Cavill R, van Herwijnen M, Coonen ML, Claessen S, et al. Extensive temporal transcriptome and microRNA analyses identify molecular mechanisms underlying mitochondrial dysfunction induced by multi-walled carbon nanotubes in human lung cells. Nanotoxicology. 2015; 9(5):624–35. DOI: 10.3109/17435390.2015.1017022 [PubMed: 25831214]

61. Grek CL, Newton DA, Spyropoulos DD, Baatz JE. Hypoxia up-regulates expression of hemoglobin in alveolar epithelial cells. American journal of respiratory cell and molecular biology. 2011; 44(4):439–47. DOI: 10.1165/rcmb.2009-0307OC [PubMed: 20508070]

62. Gross SS, Lane P. Physiological reactions of nitric oxide and hemoglobin: a radical rethink. Proceedings of the National Academy of Sciences of the United States of America. 1999; 96(18): 9967–9. [PubMed: 10468537]

63. Poynter SE, LeVine AM. Surfactant biology and clinical application. Critical care clinics. 2003; 19(3):459–72. [PubMed: 12848315]

64. Waters. [Accessed 12/30/2015 2015] Oasis Sample Extraction Products. 2015. http://www.waters.com/waters/en_US/Oasis-Sample-Extraction-Products/nav.htm?cid=513209&locale=en_US

Author Manuscript Author Manuscript Author Manuscript Author Manuscript

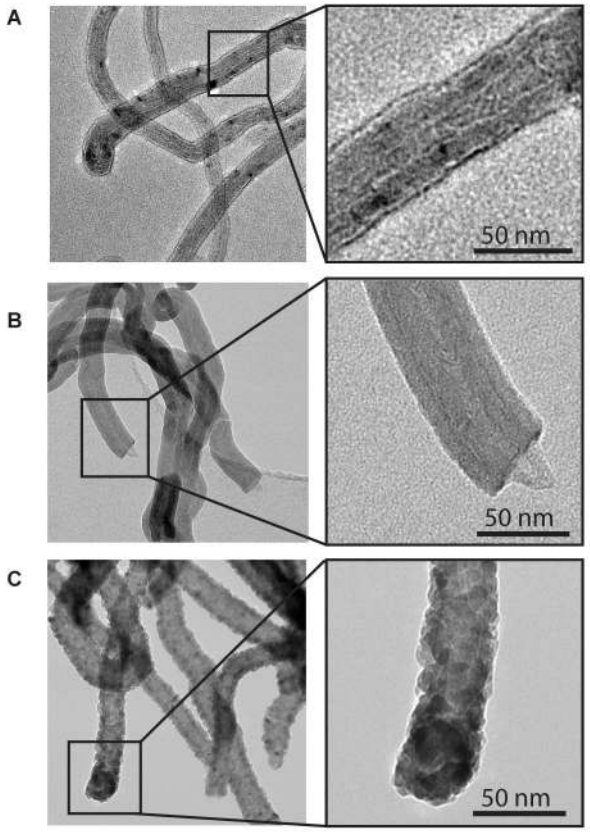

Figure 1.

Transmission electron microscopy (TEM) of uncoated MWCNTs and ALD-coated MWCNTs. **(A)** Uncoated (U)-MWCNTs. **(B)** Al_2O_3-coated (A)-MWCNTs. **(C)** ZnO-coated (Z)-MWCNTs. 50 cycles of ALD were applied to A-MWCNTs and Z-MWCNTs.

Author Manuscript Author Manuscript Author Manuscript Author Manuscript

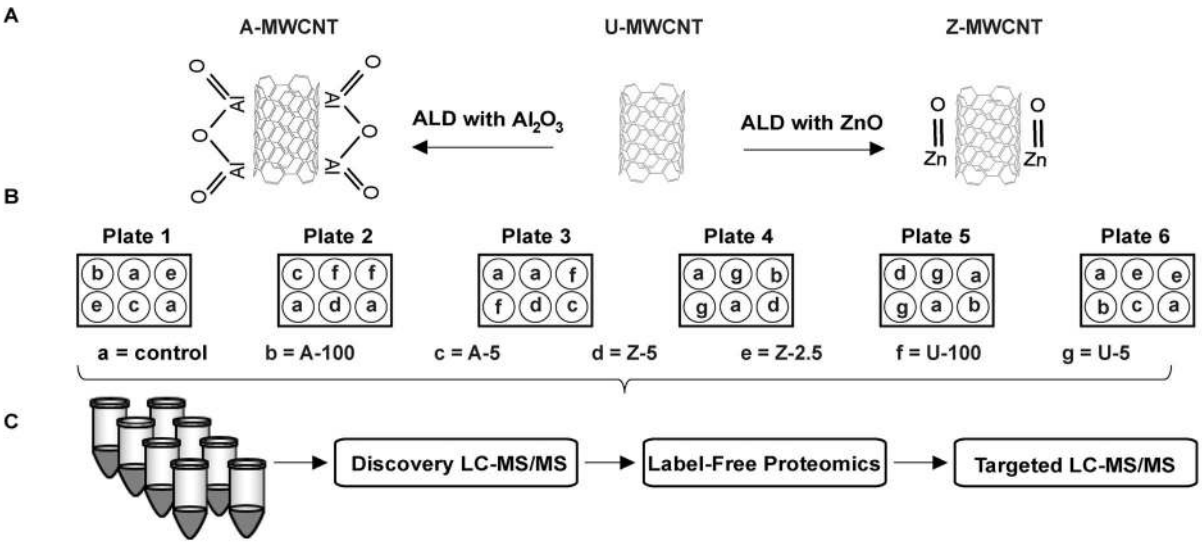

Figure 2.

(A) Atomic layer deposition with Al_2O_3 or ZnO applied to uncoated (U)-MWCNT to derive A-MWCNT or Z-MWCNT, respectively. **(B)** E10- mouse alveolar epithelial cell exposure via Latin square block design. For treatment groups a-g cells were exposed to PBS (control) or MWCNT (U, A, or Z) at the indicated doses (2.5, 5, 100) expressed in μg/ml [64]. **(C)** Proteomic sample preparation through the following steps: SDC detergent treatment to isolate proteins, peptide generation from trypsin digestion, and sample cleanup with cation exchange MCX columns. All samples were processed on the following ThermoScientific LC-MS/MS instruments: Q-Exactive Plus (Discovery) and Quantiva (Targeted).

Author Manuscript Author Manuscript Author Manuscript Author Manuscript

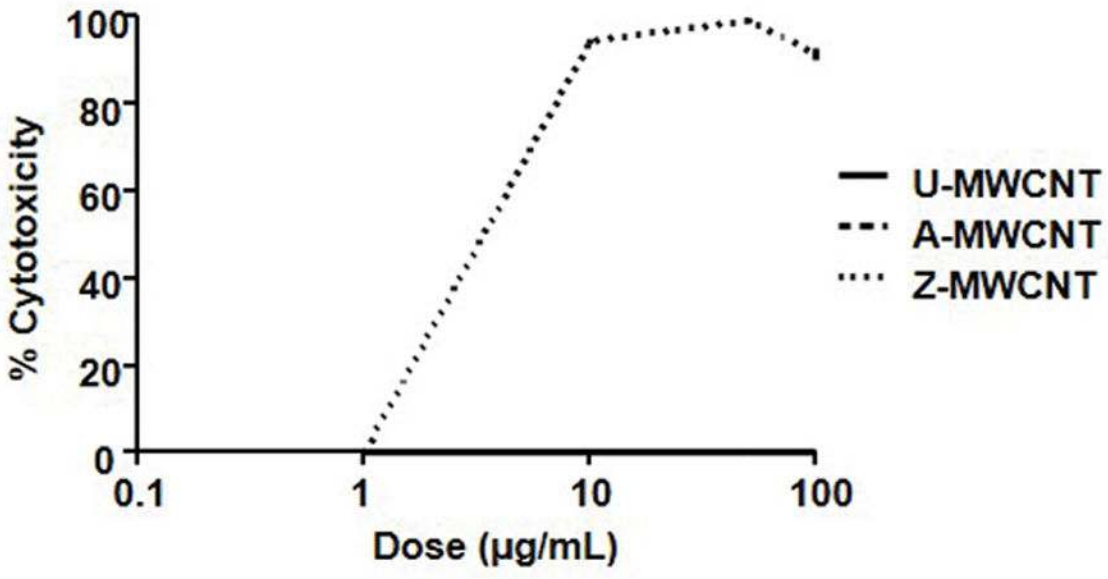

Figure 3.

Log_{10} LDH dose response of E10 cells to the following exposures: U-MWCNT, A-MWCNT, and Z-MWCNT.

Author Manuscript Author Manuscript Author Manuscript Author Manuscript

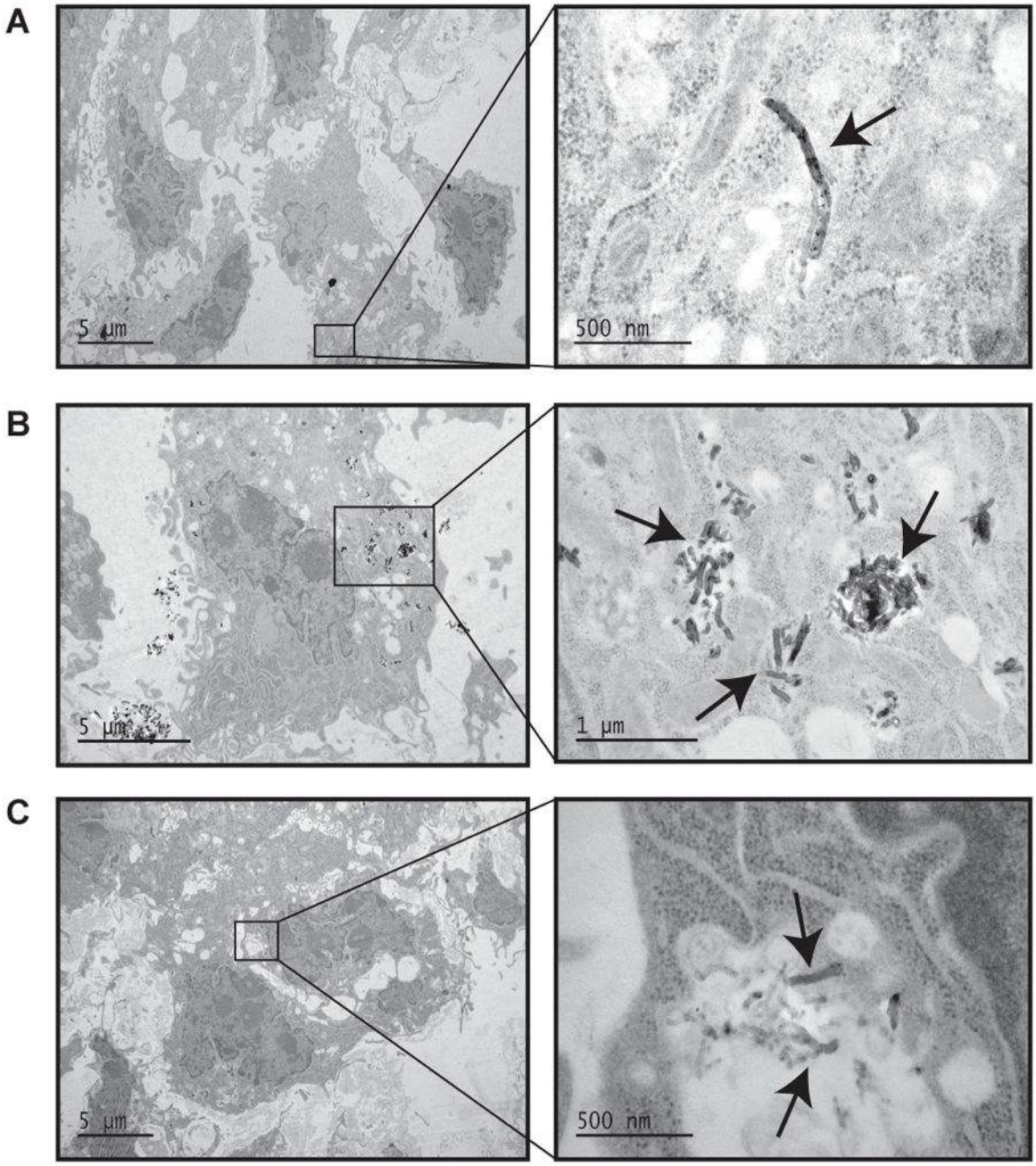

Figure 4.

TEM images of E10 cell exposure. **(A)** 5 μg/mL U-MWCNT exposure, **(B)** 5 μg/mL A-MWCNT, and **(C)** 1 μg/mL Z-MWCNT. Arrows indicate MWCNTs within the cytoplasm of E10 cells.

Author Manuscript Author Manuscript Author Manuscript Author Manuscript

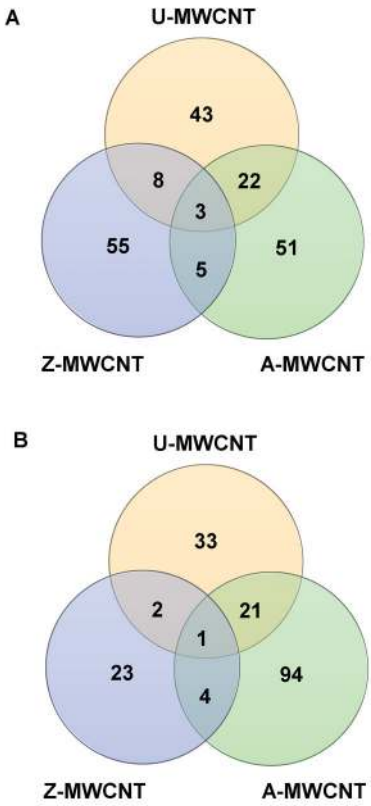

Figure 5.

Venn diagram of significant proteins by expression. **(A)** All significant proteins with increased expression compared to control. Common proteins include: hemoglobin subunit beta, hemoglobin subunit gamma, and proteolipid protein 2. **(B)** All significant proteins decreased expression compared to control. The common protein for decreased expression is fatty acid synthase.

Author Manuscript Author Manuscript Author Manuscript Author Manuscript

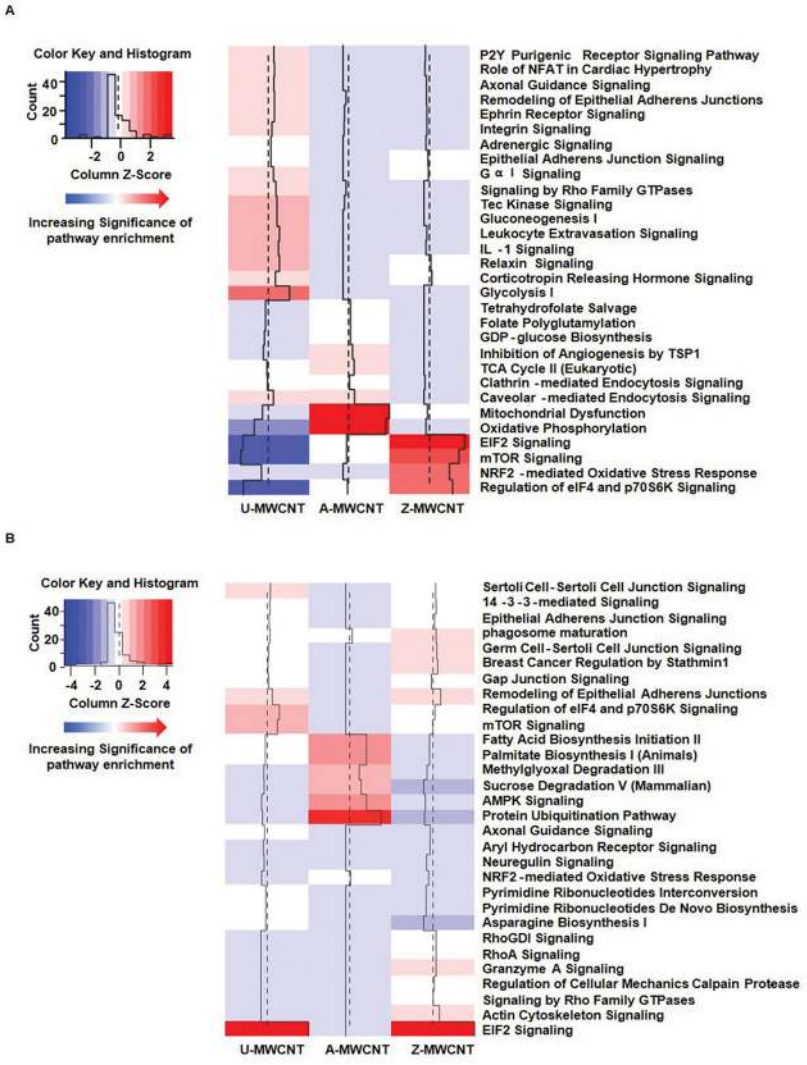

Figure 6.

Heat map of top 30 enriched pathways upon exposure to MWCNTs. Increasing significance shown from blue to red (red being the most significant). **(A)** Significant pathways corresponding to proteins with up-regulated expression upon exposure to control, and **(B)** Significant pathways corresponding to proteins with down-regulated expression upon exposure to control. A-MWCNT (aluminum oxide MWCNT compared to control), Z-MWCNT (zinc oxide MWCNT compared to control), and U-MWCNT (uncoated MWCNT compared to control).

Author Manuscript Author Manuscript Author Manuscript Author Manuscript

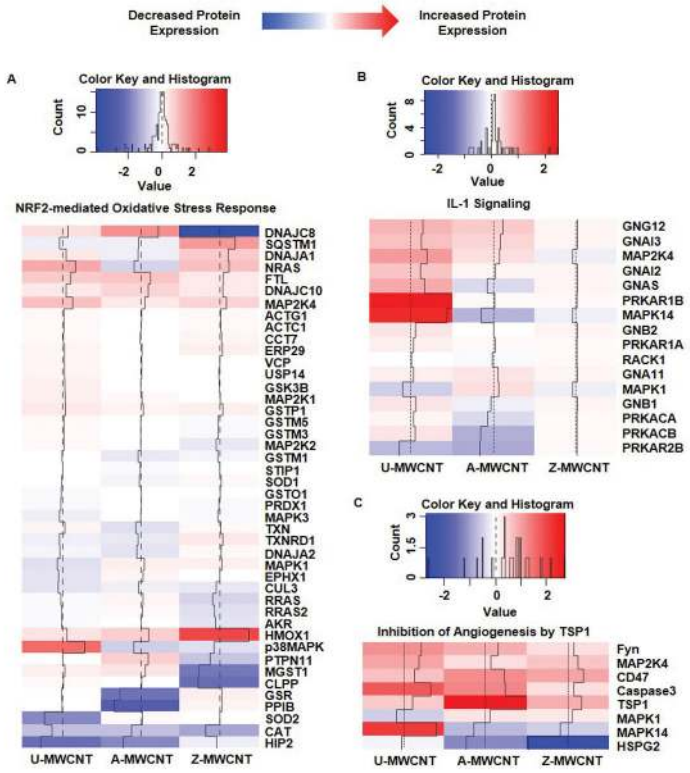

Author Manuscript Author Manuscript Author Manuscript Author Manuscript

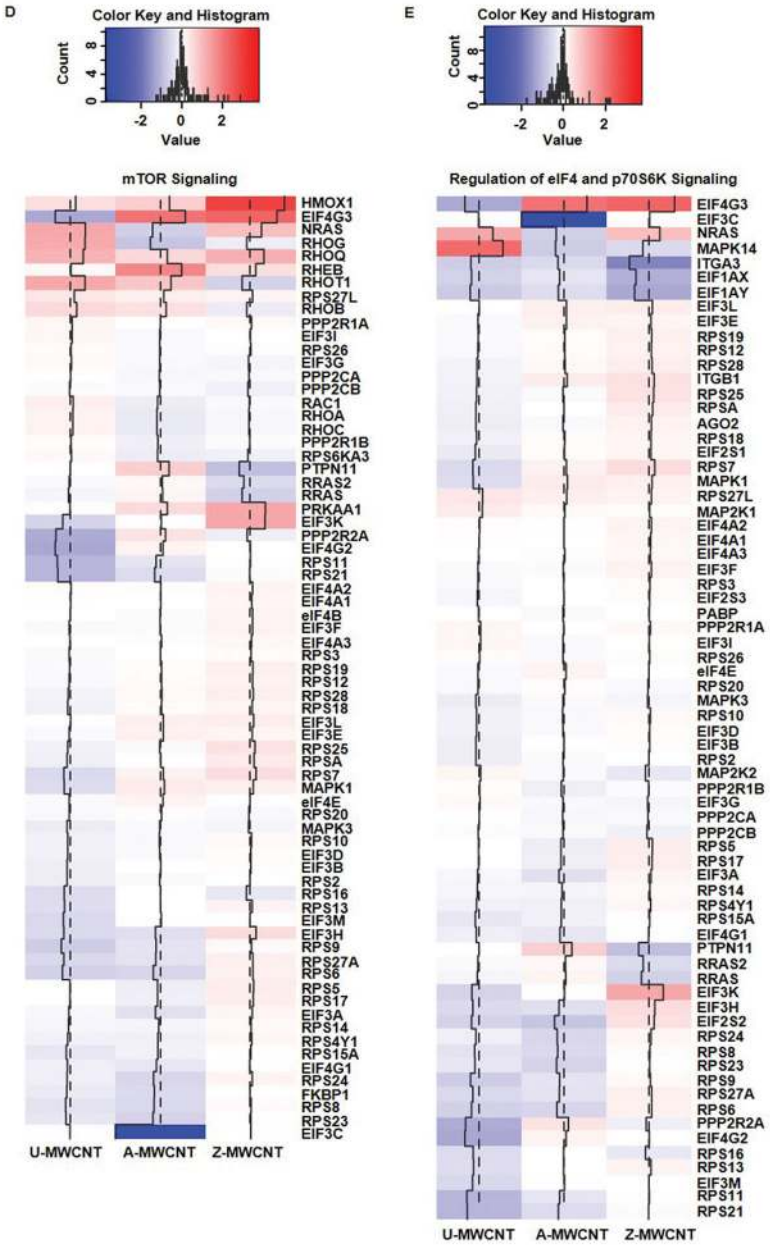

Author Manuscript Author Manuscript Author Manuscript Author Manuscript

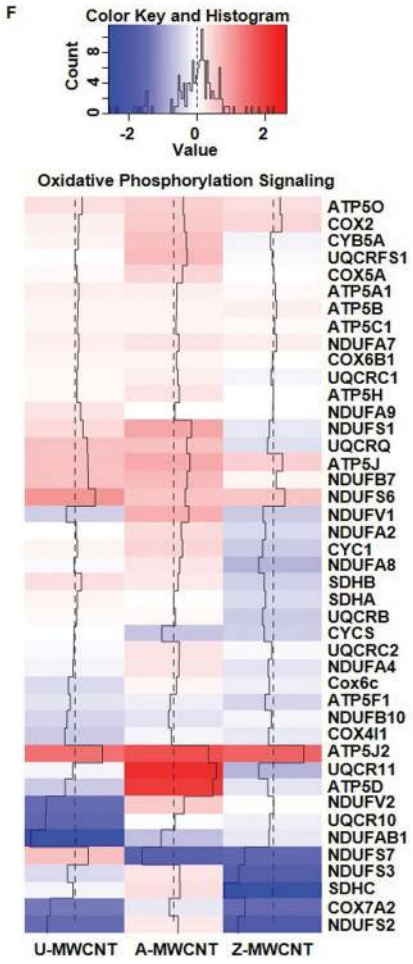

Figure 7.

Heat maps of $\log_2$ fold change for proteins of MWCNT exposed compared to control for the following pathways of interest: **(A)** Nrf-2 mediated oxidative stress response, **(B)** IL-1 signaling, **(C)** Inhibition of angiogenesis by TSP1, **(D)** mTOR signaling*, **(E)** eIF4/p70S6K signaling*, and **(F)** Oxidative phosphorylation. Log_2 fold changes in protein abundance can be read as: increased expression compared to the control (Red), and decreased expression compared to the control (Blue). *Outliers removed for higher resolution of heat map scaling. Supplemental Table 7 provides full list of proteins and $\log_2$ fold change values.